Maximum entropy model reveals frequent brain state switching in psychotic disorders in a multiversal brain function analysis

Nicholas Theis[1], Jonathan Rubin[2], Ella O'Rourke[1], Jyotika Bahuguna[3], Joshua Cape[4], Bowei Ouyang[1], Satish Iyengar[5], Konasale M. Prasad[1, 6, 7]

[1]Department of Psychiatry, University of Pittsburgh School of Medicine, Pittsburgh, PA 15213

[2]Department of Mathematics, University of Pittsburgh Kenneth Deitrich School of Arts and Sciences, Pittsburgh, PA 15213

[3]Department of Neuroscience, Laboratoire de Neurosciences Cognitive et Adaptive, University of Strasbourg, Strasbourg, France

[4]Department of Statistics, University of Wisconsin, Madison, Wisconsin

[5]Department of Statistics, University of Pittsburgh Kenneth Deitrich School of Arts and Sciences, Pittsburgh, PA 15213

[6]Department of Bioengineering, Swanson School of Engineering, University of Pittsburgh, Pittsburgh PA 15213

[7]VA Pittsburgh Healthcare System, Pittsburgh, PA 15240

*Corresponding author:
Western Psychiatric Institute and Clinic
3811 O'Hara Street
Pittsburgh, PA 15213, USA
KMP8@pitt.edu

Link to Supplement: HCP_MEM_Paper_Supplement.docx

Abstract

Background: Regional activation and pairwise correlation are mainstay neuroimaging methods. Yet, neither approach fully captures how brain networks evolve and interact over time. The maximum entropy model (MEM), which integrates regional and inter-regional activity, represents a promising integrative approach to examine dynamically evolving functional networks.

Methods: *Activation-only, pairwise-coactivation-only* analyses and an MEM framework were applied to the Human Connectome Project-Early Psychosis (HCP-EP) dataset (109 patients, 56 controls). Using the 360-node HCP/Glasser atlas to define brain regions from the default mode (DMN) and dorsal attention (DAN) networks, group differences were quantified in nodal frequency band power, functional connectivity (FC), and MEM features such as transition rates between basins in energy landscapes and their associations with cognitive and psychopathological measures were examined.

Results: Psychosis was associated with reduced first-order BOLD frequency band power and FC graph metrics. Findings specific to the MEM demonstrated a wider variety of DMN and DAN activation/deactivation patterns, with more frequent switching between them during the resting state in psychosis. Network configuration differences were more pronounced in sub-systems comprised of both DMN and DAN nodes. While BOLD frequency band power of a few regions correlated with working memory, none of the graph metrics correlated. However, basins transitions and energy correlated negatively with working memory.

Conclusion: MEM provides unique information unavailable from other analyses. Results converge among first-order-only, second-order-only, and MEM analyses, suggesting attenuated inter-network connectivity with less stability of DMN and DAN brain states in psychosis. Such changes may underlie cognitive impairments, specifically basin transitions rates in psychosis.

Key Words: fMRI; Dynamical system; functional connectivity; frequency band power; default mode network; dorsal attention network; psychosis

1. Introduction

Brain network dysconnectivity has been proposed to underlie psychotic disorders(1). Functional magnetic resonance imaging (fMRI)-based studies have reported several important findings in psychosis(2-5) with considerable variability in findings(6). A "multiversal" approach can reduce such variabilities and improve interpretability(7,8), meaning the application of complementary methods in parallel to validate findings within a sample(9). We examined the nodal activity in the blood oxygenation level dependent (BOLD) signal frequency domains, the inter-nodal functional connectivity (FC), and the systems-level maximum entropy model (MEM)-based features in the Human Connectome Project-Early Psychosis (HCP-EP) sample(10).

In the frequency domain, the most relevant fMRI signal components are the slow oscillations between 0.01 and 0.1 Hz(11). Changes in these slow oscillations better reflect coordinated neural activity(12) via neurovascular coupling and the hemodynamic response(13) due to local changes in magnetic susceptibility(14) . There are five canonical fMRI frequency bands in the BOLD signal, namely slow-5 (0.01 Hz-0.027 Hz), slow-4 (0.027-0.073 Hz), slow-3 (0.073-0.198 Hz), and slow-2 (0.198-0.5 Hz). Although a slow-1 band exists, which overlaps with the lowest frequencies of the classic delta brainwave band, slow-1 is beyond our Nyquist limit of 0.69 Hz. Slow-5 and slow-4, the slowest frequencies, have been associated with local field potential (LFP) periodicity(15) and with the hemodynamic response function(16). Slow-5 and slow-4 are widely associated with resting state networks (RSNs); some RSN properties can be shown using slow-3 and slow-2 correlations(17), but slow-3 is typically partially filtered out to completely exclude slow-2, as the latter is known to include respiratory artifacts which occur at around 0.3 Hz(18). Studies that combine fMRI with electrophysiology(19) have shown that the strength of these slow BOLD fluctuations can track the envelope of the LFP power, especially in higher frequency gamma band(20,21).

In schizophrenia, altered BOLD activity is proposed to reflect altered electrophysiological changes(22). Prior studies have found changes in power across specific resting-state frequency bands and reduced gamma activity and signs of altered neurovascular coupling in schizophrenia(23). These findings suggest disruptions in the timing and coordination of neuronal activity which are the primary features of interest in FC analysis. The latter has led to the identification of default mode network (DMN)(24) which is now acknowledged to play a role in both resting state *and* task activity(25). The DMN is central to many aspects of human cognition(24); it's disruption has been associated with schizophrenia(9). Importantly, lower frequency bands have been associated with reduced power in schizophrenia compared to controls for DMN regions(26).

Another widely studied system, the dorsal attention network (DAN), also known as the “top-down” attention network, which is altered in schizophrenia during attention-requiring tasks(27), may be responsible for attentional deficits considered intrinsic to schizophrenia(28,29). The DAN supports distinct brain functions compared to the DMN, and the two networks are often anticorrelated(30,31). While the DMN may be involved in self-referential thinking, planning, retrospection, and prospection, the DAN is associated with hierarchical management of external stimuli and goal orientation. Altered interaction between the DMN and DAN may explain cognitive impairments and psychopathology in schizophrenia(32).

Examination of regional BOLD signal differences, often called first-order analyses(33,34), and brain network connectivity analyses, referred to as second-order analysis, (35) have led to a better understanding of psychosis, but these methods are limited when considering the systemic and inherently dynamic nature of brain activity(35,36). Here, we apply first-order, second-order, and pairwise maximum entropy model (MEM) that simultaneously considers first- and second-order terms to the HCP-EP fMRI cohort. The MEM, rooted in statistical physics, is a mathematical framework applicable to multivariate time-series data(37,38). We hypothesized that MEM-derived features would provide new insights into the dynamic interactions within and between the DMN and DAN. Additionally, we examined DMN+DAN interaction at rest at the level of granularity of the HCP/Glasser atlas (39) in patients compared to controls that few studies have done.

The MEM provides novel metrics that capture temporal dynamics better than other methods given the ambiguous nature for the fMRI signal(12). These include the 1) “energy” values associated with network states via the MEM equation, which inversely relates to state probabilities (not metabolic energy); 2) the “energy landscape” analysis(37), including identifications local energy minima(40); and 3) MEM-derived statistics like basin transition rates over time and basin dwell times. We sought to determine the extent to which these quantities would differ in patients with psychosis versus controls and provide a useful new and perspective on brain pathophysiology.

2. Methods

2.1 Data Acquisition and MRI Preprocessing

We examined the T_1w anatomical MRI and the resting-state fMRI in the anterior-to-posterior encoding direction from the HCP-EP dataset(10). We applied HCP minimal preprocessing standard(41) on the Pittsburgh Supercomputing Center’s (PSC) Bridges-2 system(42). T_1w images were used as inputs to the FreeSurfer (version 7.4.1) *recon-*

all function(43), which performs intensity normalization, tissue labeling, and subcortical segmentation. The FMRIB Software Library (FSL version 6.0) was used for fMRI preprocessing(44) as described previously(45). Rigid body motion correction, head motion estimation, and TOPUP were applied to each volume.

The T_1w images were registered to EPI space, followed by aligning with the atlas. We used the 360-node HCP/Glasser cortical atlas and 17 subcortical structures(39) as described earlier(46), providing a means to create subject-specific region-of-interest atlases. Briefly, the T_1w image is down-sampled to the EPI images, followed by nearest-neighbor interpolation of the subject-specific atlas. This allows for a precise mapping of the cortical boundaries to the native EPI and obviates the need to warp or alter the EPI data into standard space. The average voxel activation at each timepoint was calculated for each region (node), producing a timeseries of fMRI activation per individual in the network.

This study uses the cortical regions as fundamental units of functioning(47). We thus do not use cluster analysis or independent component analysis but rather the above-described HCP/Glasser brain atlas to define a cortical region. The DMN and DAN have both been previously defined in this atlas and are non-overlapping. The DMN consists of 34 bilateral nodes from the posterior cingulate, anterior cingulate, and lateral parietal(48). The DAN consists of 24 bilateral nodes from the frontal, parietal, and occipital cortices (49).

2.2 First-order Analysis

For each subject and region, four canonical fMRI frequency band powers were calculated, and whole-brain patient and control band power data were compared using MANCOVA controlling for age and sex followed by examining group differences in each region using between-subjects' effects correcting for multiple tests (**Supplemental Section S.1**).

2.3 Second-order Analysis

Functional connectomes were measured from the regionally averaged fMRI timeseries using Pearson's correlation (over time) of every region-pair (network edge)(35). We examined the DMN, the DAN, and the 58-node DMN+DAN, each including those edges for which the p-value associated with the correlation strength between nodes <0.05, wherever thresholding was necessary. The Brain Connectivity Toolbox (50) was used to estimate weighted graph measures on the connected networks (where *no* threshold was applied), including nodal clustering coefficient (CC), modularity, and efficiency. Nodal betweenness centrality (BC) was calculated on binary graphs. Graph-level averages of BC and CC were calculated for each subject. All graph

measures were compared between groups using MANCOVA model controlling for age and sex followed by between-subjects' effects applying appropriate multiple test corrections. Edge weights were compared directly by group using two-sample KS tests. Frequency-band-specific FCs were also created, and graph measures compared for the four frequency bands (**Supplemental Section S.2**).

2.4 MEM Analysis

The pipeline from fMRI-to-MEM followed a previously published method(40,51). The MEM energy function includes a parameter vector *h*, corresponding to first-order node activation terms, and a parameter matrix *J,* corresponding to second-order, simultaneous activations of node-pairs. To derive these parameters, we defined state vectors of dimension equal to the number of nodes in the network, each with entries given by 1 for active node and –1 for inactive node in that state.

Concurrently, the fMRI timeseries were z-scored(52) and a threshold of zero was applied to produce a binary activity timeseries for each node. A node was considered "off" if its z-scored value was ≤0, or "on" if it was >0. For each node, over the course of each subject's fMRI (410 timepoints), the number of nodal switching events (microstate) was recorded, i.e. the number of times the node switches from off-to-on or on-to-off, going from one timepoint to the next. The number of microstate switches per node was compared across all subjects for each band. Whole-population correlations between nodal group level average band power and group level average number of nodal microstate switch events were examined. Within-group correlations were also calculated across subjects for each node and compared per band. Within-group ANOVA models were run to test the association of band power and microstate switching. Finally, the number of microstate switches was ranked by node, and the population distributions were compared by group using Kolmogorov–Smirnov (KS) test for networks composed of the top ten nodes or bottom ten nodes in terms of switching frequency.

Binary state probabilities were calculated at the full sample level, by concatenating all subject data from that population. The number of distinct binary states observed per subject was calculated for each collection of nodes (see next section), and distributions of numbers of distinct states were compared by group using the two-sample KS test. Finally, we used maximum-likelihood estimation to estimate the MEM parameters, *h* and *J*, for each population according to the observed group-level average node activity level and pair-wise correlations of the nodes.

This procedure was repeated for 6 different collections of nodes, namely the most (top) and least (bottom) frequently state-switching DMN, DAN, and DMN+DAN nodes. After model fitting, for each of the six systems, the binary state time series for each participant's fMRI (across 410 timepoints) was converted to an energy timeseries, based on the MEM energy values as the subject's energy trajectory. The sum of the

energies of the states of this trajectory is the “energy trace.” The trajectory is time-resolved, while the trace is a non-time-resolved aggregate energy. Energy trace distributions were compared between patients and controls for the six systems using two-sample KS tests.

After estimating the MEM parameters, disconnectivity graphs of local energy minima of the MEM for each set of nodes was calculated based on binary Hamming distances(40). Hamming distance defines states as neighbors if they are only 1 microstate switching event apart. Within the resulting graph, a basin is associated with each state that represents a local energy minimum. Then, non-minimal states were classified as belonging to basins if the shortest neighbor-to-neighbor path from the state to the basin minimum state is decreasing in energy. These represent the conceptual paths of least resistance and may dictate which energy trajectories are observed, but in practice for real fMRI timeseries, the energy of the state at time *t+1* is not always less than the energy at time *t,* allowing the real trajectory to traverse many basins and not become “stuck” in one. Following the trajectory through a series of basins allows us to calculate the number of “basin transitions” per subject (the basin transition rate) and “basin-specific dwell times” per subject, per basin. The distribution of transition counts, and dwell times were compared by group using two-sample KS-tests for each system. The MEM analyses were done using a modified version of package *elapy* (https://github.com/okumakito/elapy/tree/main/elapy) and custom MATLAB code.

2.5 Association with cognition

We used the t tests and ANOVA to test differences in the distribution of age and sex, MANCOVA for the derivatives from first- and second-order, and MEM analyses using age and sex as covariates. We, next, examined whether these imaging-derived variables that were significantly different between groups were associated with performance on selected cognitive tests that included attention (*d’* from auditory continuous performance task, ACPT), list sorting working memory test (LSWMT), Flanker test for executive function, and age-adjusted dimensional change card sort (DCCS) test from the NIH Toolbox using partial correlation tests controlling for age, sex and diagnostic status correcting for multiple tests.

3. Results

3.1 Sample Characteristics

Our final sample consisted of 165 (109 patients and 56 controls) after excluding nine for either not having a complete cortical parcellation, failing preprocessing, or not having the expected number of timepoints (c.f. other studies included 93 to 124 patients(53-55)). Patients were younger than controls (t=3.33, p=0.0011) with no difference in sex distribution (χ^2=0.21, p=0.64) **(Table 1)**.

Group	N	Mean Age (years)	Sd Age (years)	Females	Males	Affective	Non-Aff
Controls	56	24.9	4.0	19 (34%)	37 (66%)	0	0
Patients	109	22.8	3.8	41 (38%)	68 (62%)	26	83
Schizophrenia	58	24.93	4.00	19	39		
Schizoaffective d/o	14	22.17	3.40	4	10		
Schizophreniform d/o	6	24.71	4.28	2	4		
Delusional d/o	1	23.17		1	0		
Brief psychotic d/o	1	30.75		1	0		
Psychosis NOS	3	23.41	5.33	0	3		
Major depressive d/o	20	21.50		12	8		
Bipolar disorder	22	24.14	4.30	8	14		

Table 1. Clinical and demographic data (some participants may have more than one diagnosis as these are lifetimes rates)

3.2 First-Order Results

A MANCOVA model with all 377 regions was significant (Wilk's λ=0.01, F=354.14, p=0.04). Posthoc between-subjects' effects correcting for multiple tests using Bonferroni method showed that regional frequency band power in all four frequency bands was lower in patients compared to controls in 215 out of 377 regions.

Within the DMN and DAN, 13 of the 58 regions showed significantly reduced BOLD frequency power in a MANCOVA model (Wilk's λ=0.50, F(58,104)=1.81, p=0.004)(Posthoc between-subjects' effects, Bonferroni corrected p, all<0.02) (**Figure 1**).

3.3 Second Order Results

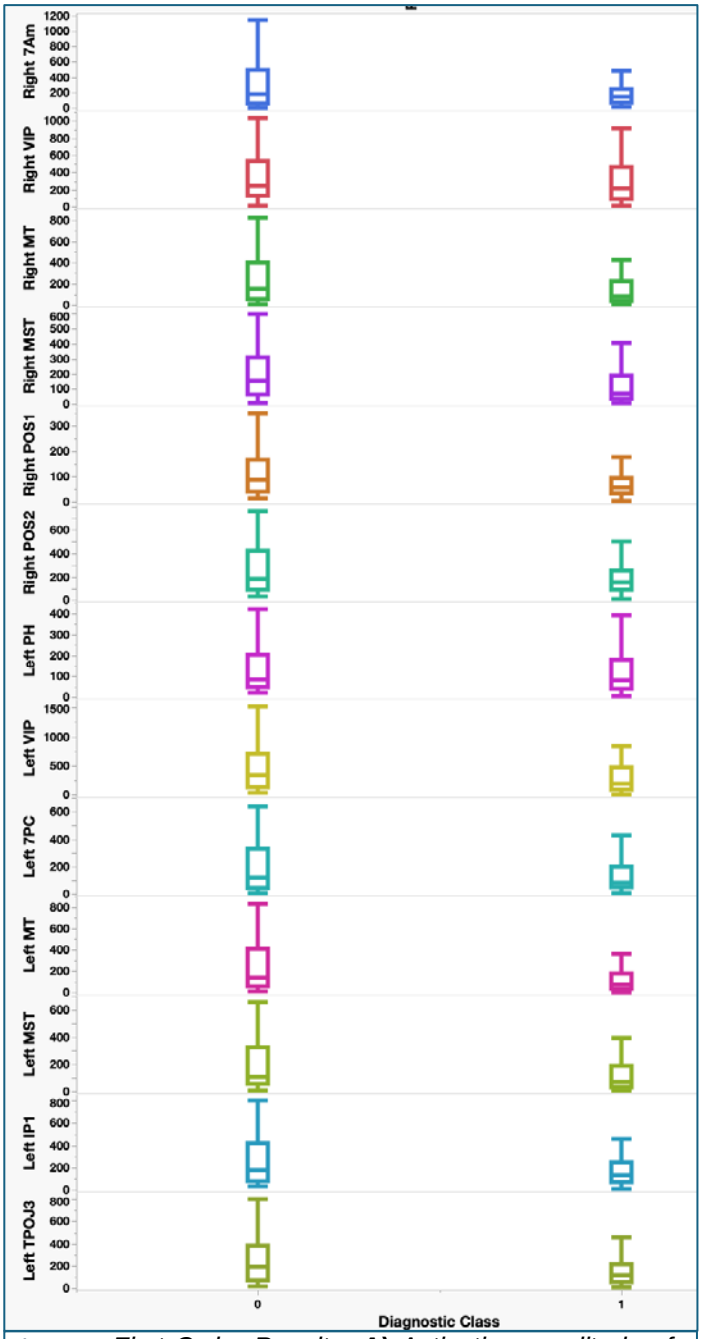

Figure 1: First Order Results. ***A)*** *Activation amplitudes for 13 of the 58 DMN and DAN regions that showed significant differences between early psychosis patients (1 on x-axis) and healthy controls (0 on x-axis). Average activation of the regions (raw BOLD signal value over time) per group are plotted in the box plots with standard error bars.*

separate band **(Supplemental Section S.2**).

From 34 DMN nodes and 24 DAN nodes, a 58-node network representing a combined DMN+DAN complex was made for each subject. The average FC for the DMN+DAN is in **Figures 2A and B.** Of the 1,653 individual KS-tests performed for groupwise differences in edge weight (one for each unique edge in the 58-node network), 181 (about 10% of edges) demonstrated different edge weight distributions between groups at the alpha=0.001 with more negatively weighted edges in patients (**Supplemental Section S.2**).

Network connectivity measures calculated for the entire 58-node DMN+DAN network, as well as the 34-node DMN and 24-node DAN. MANCOVA model controlling for age and sex with all these measures was significant (Wilk's λ=0.94, F(4,158)=0.046) (Posthoc between-subjects' effects with Bonferroni correction, $p<0.015$ for all measures) (**Table 2**). The same patterns were exhibited when frequency-band-specific FC networks were made, except in slow-2, which was similar between groups and had weaker connections network-wide compared to slow-5; similarly, DMN-only and DAN-only FC network properties were examined between groups for each

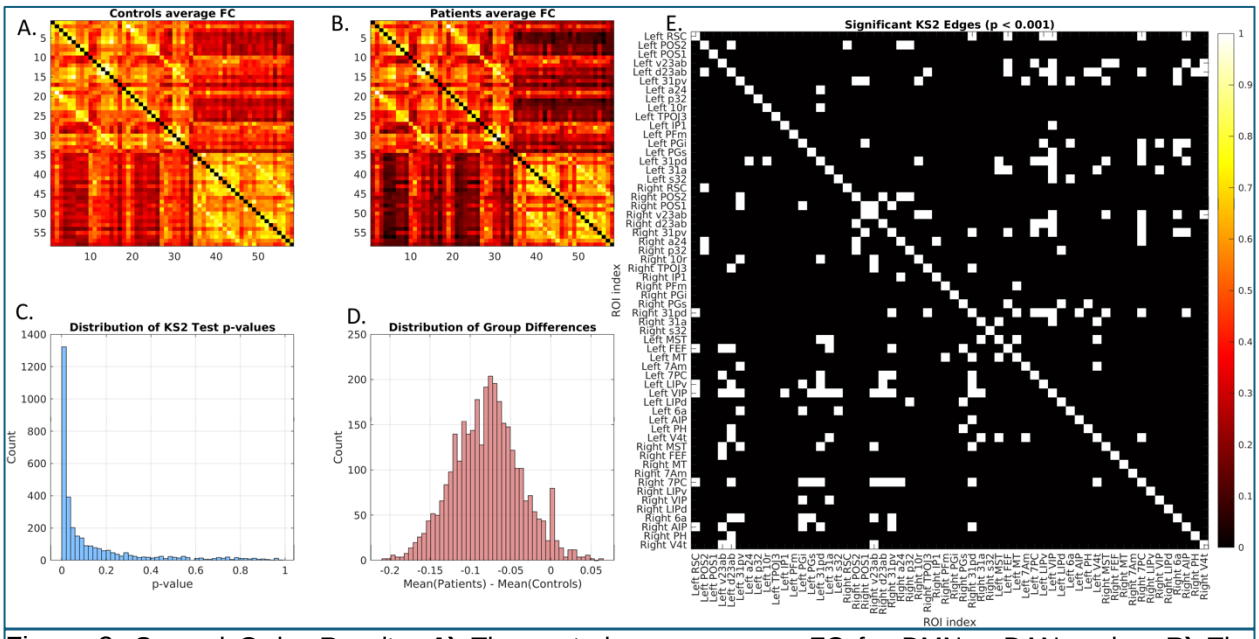

Figure 2: Second Order Results. **A)** The control-group average FC for DMN + DAN nodes. **B)** The patient-group average FC for DMN + DAN nodes. **C)** Histogram of p-values for two-sample KS-test of FC edge weight distribution by group over all tests (upper and lower triangle). **D)** Histogram of difference in group level average edge weight. **F)** The binary outcome of null hypothesis rejection at level alpha 0.001 for the two-sample KS-test by edge.

		DMN		DAN		DMN+DAN	
Metric	**Group**	**Mean**	**SD**	**Mean**	**SD**	**Mean**	**SD**
Clustering	Controls	**0.41	0.09	**0.49	0.14	**0.36	0.11
	Patients	**0.36	0.11	**0.43	0.13	**0.30	0.11
Modularity	Controls	**0.07	0.03	0.06	0.04	**0.12	0.05
	Patients	**0.09	0.03	0.07	0.04	**0.15	0.06
Efficiency	Controls	**0.47	0.08	**0.53	0.11	**0.43	0.09
	Patients	**0.42	0.09	**0.48	0.11	**0.39	0.09
Betweenness	Controls	23.37	11.12	12.02	9.36	**54.35	27.54
	Patients	26.61	12.57	14.03	7.80	**67.59	28.94

Table 2. Graph metrics for second-order comparisons. Asterisks indicate significance at **p<0.01.

3.4 MEM Results

MEMs were fit to concatenated binary activation state data for each of the six

systems, each consisting of ten nodes. The most frequent microstate switching (top)

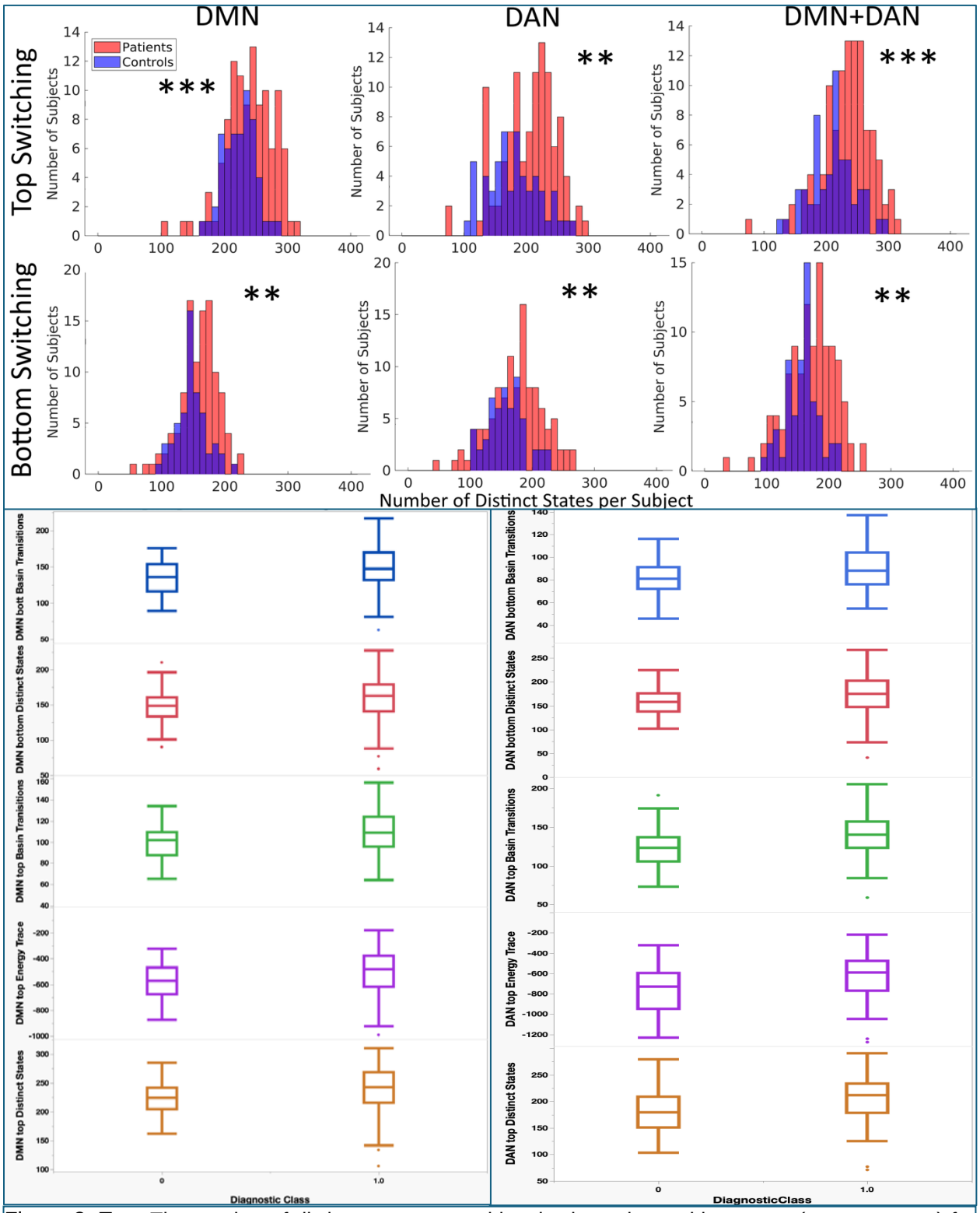

Figure 3: Top: The number of distinct states per subject is shown in two histograms (one per group) for the six systems. Asterisks indicate significance of difference of distribution by 2-sample KS-test (**p<0.01; ***p<0.001). Bottom: Differences in MEM metrics for DMN and DAN observed using MANCOVA model. Observed significances are corrected for multiple tests using Bonferroni approach (DMN+DAN differences are in supplemental information).

DMN and least frequent (bottom) DMN, the top DAN and bottom DAN, and finally the

top DMN+DAN and bottom DMN+DAN, were considered. The DMN+DAN systems had 5 nodes from each constituent system. All fits were successful (**Supplemental Material S.3**).

Across all six systems, patients exhibited more distinct states per subject (on/off states of the nodes) than controls, independent of sample size (**Figure 3**). The distributions of number of distinct states in the top DMN (*KS*=0.32, *p*<0.001), bottom DMN (*KS*=0.31, *p*=0.001), top DAN (*KS*=0.30, *p*=0.002), bottom DAN (*KS*=0.30, *p*=0.003), top DMN+DAN (*KS*=0.37, *p*<0.001), and bottom DMN+DAN (*KS*=0.30, *p*=0.001) were significant. The patients consistently exhibited more unique states than the control population in each system.

A MANCOVA model consisting of all MEM metrics (top and bottom distinct states, energy trace, basin transitions in the DMN, DAN, and DMN+DAN) was significant for patient-control differences (controlling for age and sex) (Wilk's λ=0.82, F=1.79, p=0.03). Posthoc between-subjects' effects applying Bonferroni corrections showed that all metrics (top and bottom distinct states and basin transitions, along with top energy trace of DAN, DMN, and combined DAN+DMN) were significantly higher among patients compared to controls (p<0.03), but bottom energy trace in all three systems did not show differences.

We examined differences in MEM metrics among non-affective psychosis (NAP), affective psychosis (AP) patients, and controls using MANCOVA that showed a trend toward significance (Wilk's λ=0.72, F=1.42, p=0.051). Posthoc between-subjects' effects for MEM metrics with Bonferroni corrections showed a similar pattern of significant differences in MEM metrics as psychosis-control comparison except for bottom distinct states showing a trend toward significance (p=0.08). Another posthoc test to compare NAP, AP, and controls, showed that all MEM metrics with significant differences in the between-subjects' effects tests were different between controls and NAP but not between controls and AP except top energy trace, which was the highest in NAP, intermediate in AP and the lowest in controls after Games-Howell corrections for multiple testing.

Between NAP and AP patients, no differences in the distributions of distinct states were found in any of the six systems. Between NAP and controls, differences were seen in every system (DMN-top: KS=0.33, p=0.001; DMN-bottom: KS=0.31, p=0.002; DAN-top: KS=0.30, p=0.003; DAN-bottom: KS=0.33, p-0.001; DMN+DAN-top: KS=0.34, p<0.001; DMN+DAN-bottom: KS=0.33, p<0.001). Between AP and controls, significant differences were observed in three systems (DMN-bottom: KS=0.32,p=0.037; DAN-top: KS=0.37, p=0.012; DMN-DAN-top: KS=0.448, p<0.001).

After fitting MEMs at the whole-sample level, we computed state energies, which is inversely related to state probability, and mapped each subject's binary fMRI time course to energy time series showing significant patient–control differences for top but not bottom systems: DMN top (KS=0.29, p=0.003) DAN top (KS=0.34, p<0.001) and DMN+DAN top (KS=0.33, p<0.001) (**Figure 4)**. This pattern mirrors first-order results, where group differences were present in top-switching nodes but not in bottom-switching DMN. Among comparisons of second-order metrics, the DAN showed the greatest similarity between groups.

Between NAP and AP patients, no differences in the distributions of energy trace were found in any of the six systems. But there were differences between NAP and

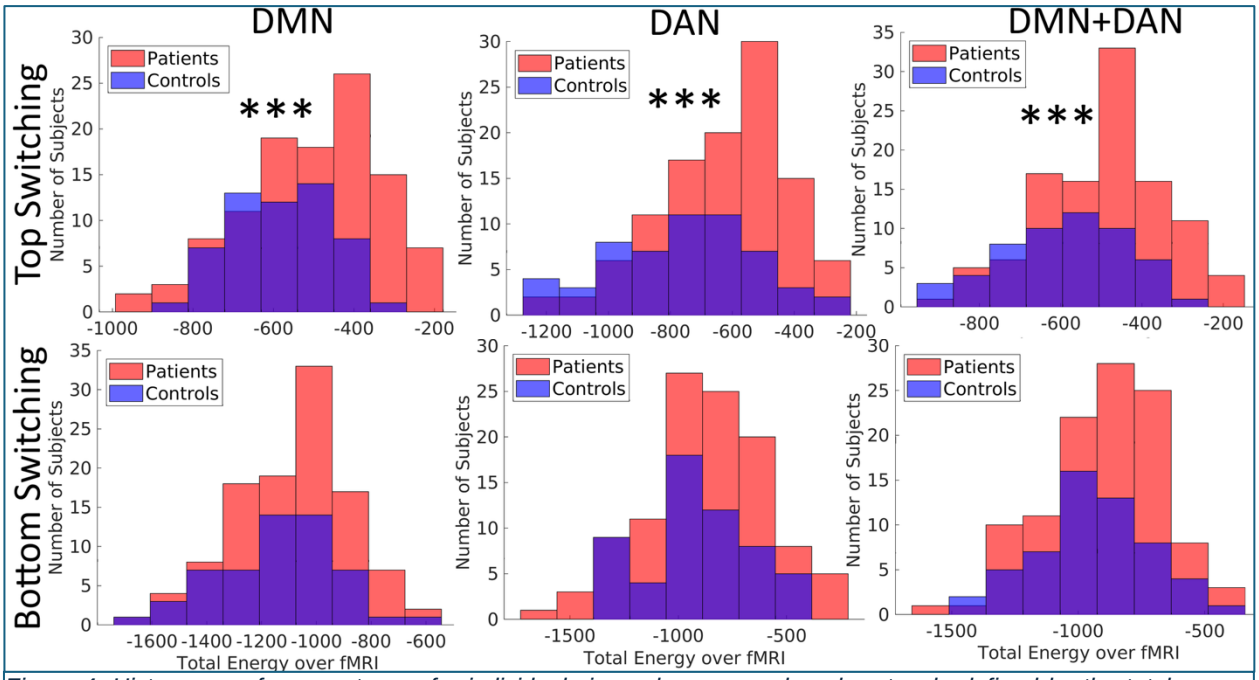

*Figure 4: Histograms of energy traces for individuals in each group and each network, defined by the total energy values across all observed states per subject. The figure shows that the patients have higher traces than controls in the top switching systems. Two-sample KS-test: **p<0.01; ***p<0.001.*

controls in two systems (DAN-top: KS=0.35, p<0.001; DMN+DAN-top: KS=0.34, p<0.001). Between AP and controls, DMN-DAN-top energy trace showed significant differences (KS=0.32, p<0.038).

For each network, a single MEM was fit to combined patient and control data, yielding a shared energy landscape on which all subjects' state trajectories could be compared (**Figure 5**). Basin structure differed by the system: the bottom-switching DMN showed a complex landscape, whereas the top-switching DMN was dominated by all-on and all-off states; the DAN showed the opposite but weaker pattern. Across all six systems, the all-on and all-off basins were dominant. In the combined DMN+DAN networks, additional basins corresponding to DMN-only and DAN-only activation indicate dynamic alternation between co-activation, co-deactivation, and mutually

exclusive states possibly resulting from the anti-correlational nature of the two constituent networks (**Figure 2**).

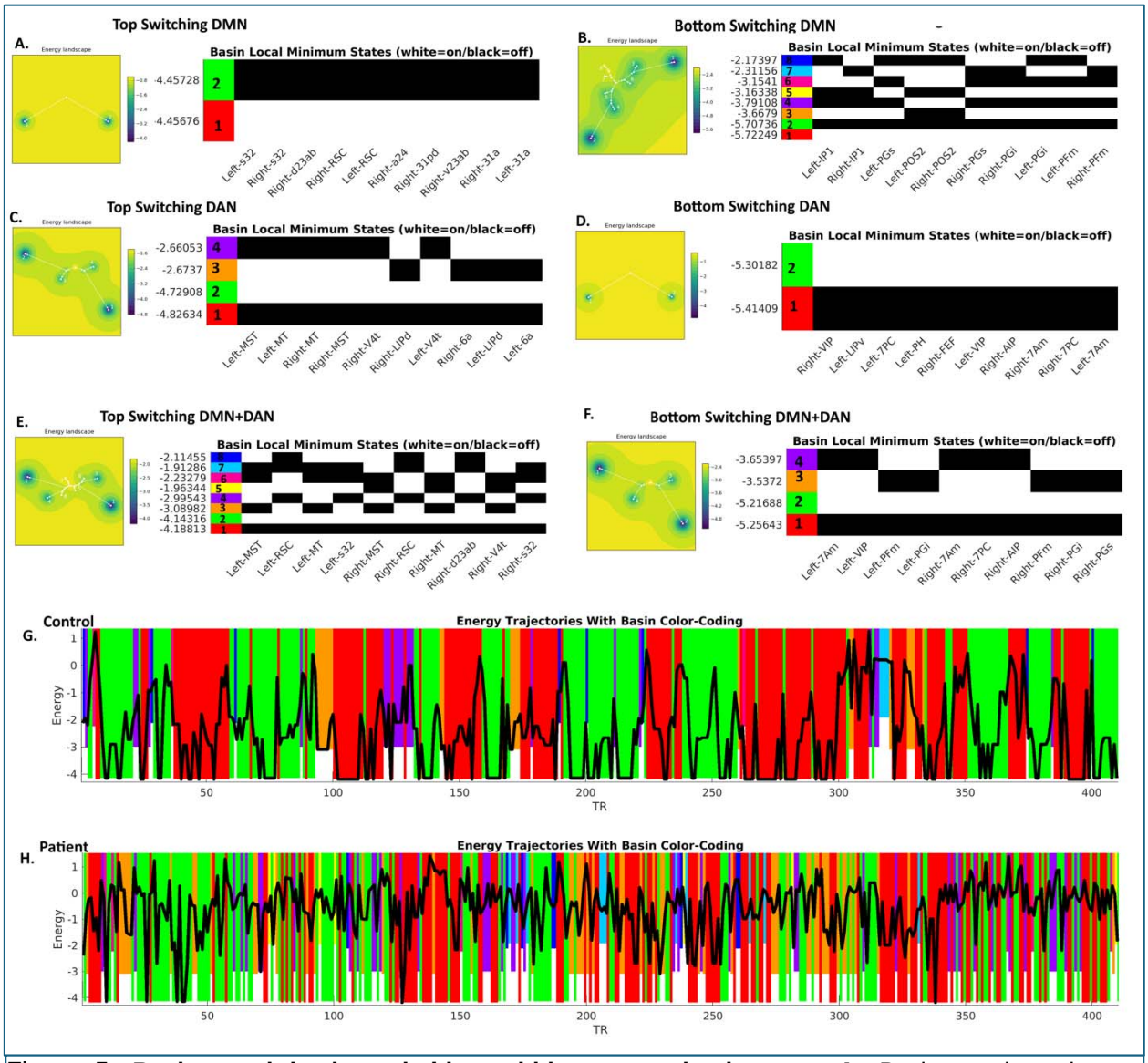

Figure 5: **Basins and basin switching within energy landscapes. A.** Basin graph and state configurations for basins for top switching DMN. **B.** Basin graph and state configuration for basins for bottom switching DMN. **C.** Basin graph and state configuration for basins for top switching DAN. **D.** Basin graph and state configuration for basins for bottom switching DAN. **E.** Basin graph and state configuration for basins for top switching DMN+DAN. **F.** Basin graph and state configuration for basins for bottom switching DMN+DAN. **G**. The color-coded (by basin) energy trajectory for the 410 fMRI timepoints in an example control subject. **H.** The color-coded (by basin) energy trajectory for the 410 fMRI timepoints in an example patient. Both **G** and **H** use the basin color coding given in **E** and represent an example participant's top switching DMN+DAN. Thick black line represents energy value; colored rectangle represents occupation of corresponding basin; rectangle height represents basin depth. Note that colors do not correspond between systems but are in the same order for all systems (i.e. red is always identifies the system's lowest energy basin).

Basin transition counts differed between groups (**Figure 6**), being significant for top-switching DMN (KS=0.30, p=0.002), DAN (KS=0.32, p<0.001), DMN+DAN (KS=0.36, p<0.001), and bottom switching DMN+DAN (KS=0.33, p<0.001). Patients had more state transitions overall, but the transition rates between specific basins were the same (**Supplemental Section S.4**), indicating that patients had *more* basin transitions but *not* different temporal transition patterns. Interestingly, direct transitions from a DMN-exclusive state to a DAN-exclusive basin (or vice versa) were infrequent (<5%), compared to a high probability of staying in an exclusive basin (~40%), or transition from the all-nodes-on to all-nodes-off basin (~15%). In the DMN+DAN networks, the lowest-energy basins corresponded to DMN-only or DAN-only activation (basins 3 and 4 in **Figure 5E,F**). Direct switches between these basins were minimal (2-4%, **Supplemental Section S.4**), suggesting that DMN and DAN nodes switch largely independently under the resting state condition.

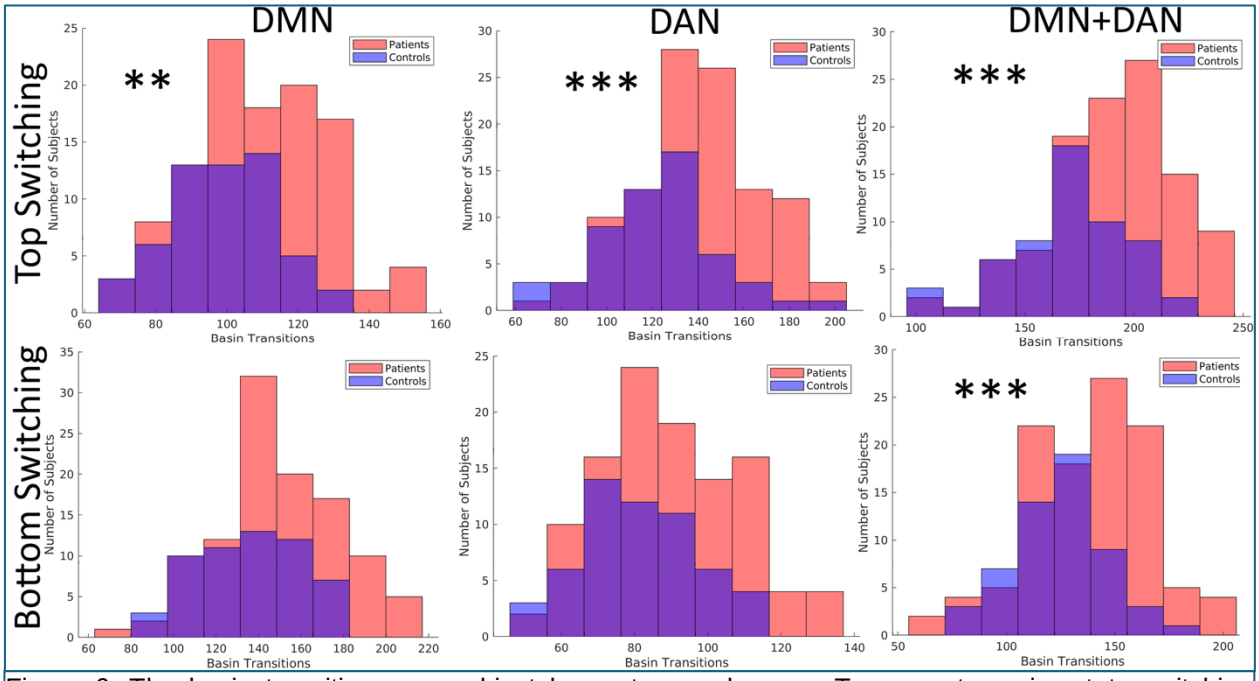

Figure 6: The basin transitions per subject by system and group. Top row: top microstate switching networks, bottom row: bottom microstate switching networks. From left to right: DMN, DAN, DMN+DAN. Asterisks indicate significance level of difference of distribution by two-sample KS-test: **p <0.01; ***p <0.001.

the distributions of basin transitions states were found in any of the six systems. Between NAP and controls, differences were observed in every system (DMN-top: KS=0.36, p<0.001; DAN-top: KS=0.35,p<0.001; DMN+DAN-top: KS=0.38, p<0.001; DMN+DAN-bottom: KS=0.36, p<0.001) after correcting for multiple tests.

In addition to basin energies and transition frequencies, average dwell time per participant was calculated for each basin and compared between groups (**Figure 7**).

Some basins showed significantly shorter dwell times in patients, while others were similar across groups. In the top-switching DMN+DAN system, basin 1 (all-off) and basin 3 (DMN-only) had shorter dwell times in patients. In the bottom-switching DMN+DAN, patients also had shorter dwell times in the all-on and DAN-only basins (2 and 3, respectively).

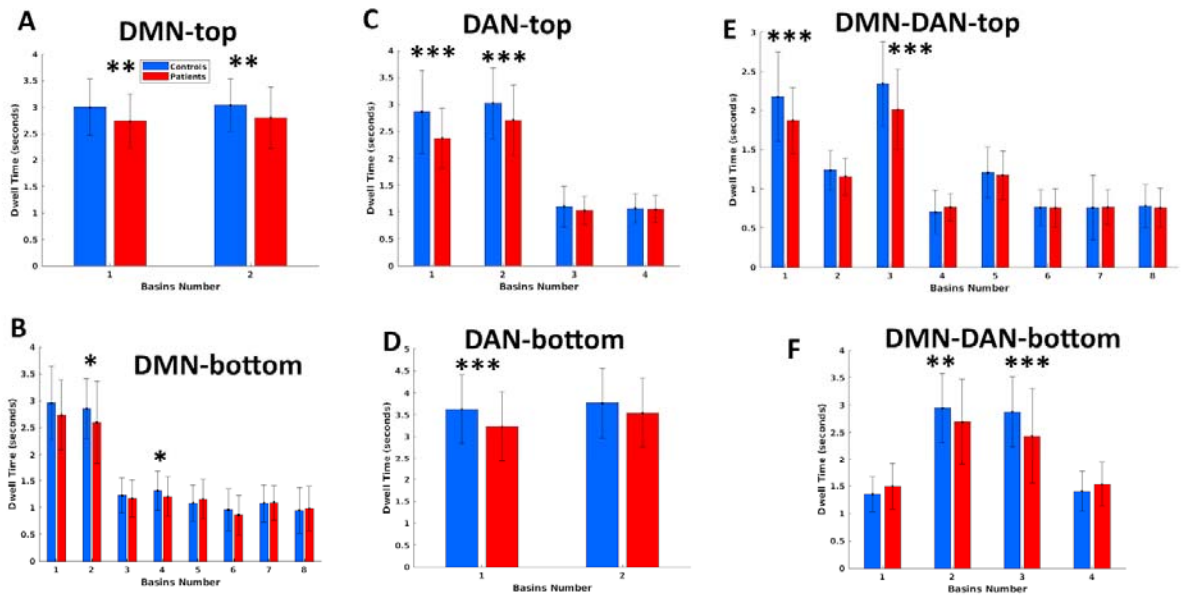

Dwell Times	Basin 1	Basin 2	Basin 3	Basin 4	Basin 5	Basin 6	Basin 7	Basin 8
DMN-t	.29**	.29**						
DMN-b	.19	.24*	.19	.25*	.21	.08	.14	.10
DAN-t	.34***	.27**	.13	.10				
DAN-b	.34***	.19						
DMN-DAN-t	.31***	.20	.34***	.08	.11	.09	.09	.14
DMN-DAN-b	.17	.30**	.39***	.14				

Figure 7: KS-tests for basin dwell times between groups. Values are KS-statistics, asterisk indicates significance of KS-test: *p <0.05, **p <0.01, ***p <0.001 (survives Bonferroni corrections). In every case where significance was detected, the patients always had a lower average dwell time for the basin. A variable number of basins was detected per system; where cells are grey (blank), the system did not have that many basins.

3.5 Relationship among first-order, second-order, and MEM results

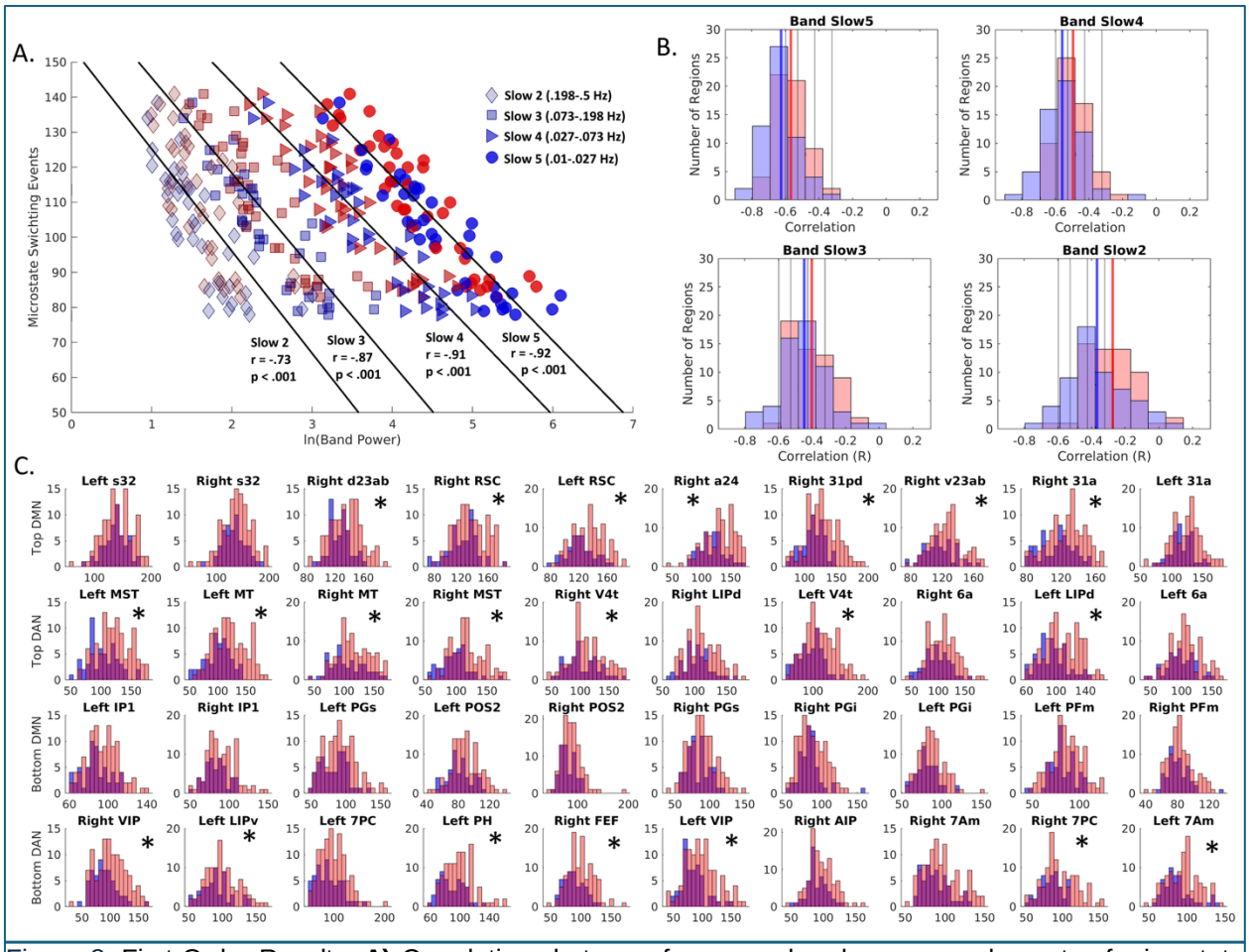

Figure 8: First Order Results. **A)** Correlations between frequency band powers and counts of microstate switching events, where each point represents the group-level average (controls in blue, patients in red) for a region. **B)** Distributions across subjects of correlations between switching and power, for each band, by group. Black vertical lines show band averages from all bands (including subplot plots), whereas blue and red vertical lines show control and patient (respectively) group level average correlations (of regions) for that subplot. Histograms show nodal distributions of correlations calculated across subjects within a group. **C)** Micro-switching by group: asterisks indicate significant differences in patient-control distributions by KS-test after FDR correction at alpha = 0.05. For both DMN and DAN, the top (most microstate switching events) and bottom (least microstate switching events) 10 regions are shown. Histograms represent all individuals, where y-axis is number of participants and x-axis is number of microstate switching events in the given region over the course of the resting state fMRI acquisition.

We observed a significant negative association between microstate switching and band power in every power band. The group level average band power of the number of region-wise microstate switching events and the group level average band power are shown as scatter plots in **Figure 8A.** At faster frequency bands, negative association is relatively weaker, suggesting that power in higher frequency bands, which are typically associated with respiratory artifacts (slow-3 and slow-2), is less associated with microstate switching compared to slower frequency bands (slow-5, slow-4), which are strongly associated with microstate switching, whereas slow-3 and slow-2 are less strongly associated with microstate switching (**Figure 8B**). From both whole-population

and within-group ANOVA tests (**Supplemental Section S.1**), all post-hoc F-tests were significant at level $p<0.001$.

Among the top and bottom 10 DMN and 10 DAN (40 unique nodes), 21 were found to have significant differences in microstate switching frequency between patients and controls **(Figure 8C).** Patients, on average, had more microstate switching at the group average level, and notably no differences were observed in the bottom (least frequent) microstate switching DMN nodes.

3.6 Associations with cognitive functions and psychopathology severity

Cognitive performance: We selected cognitive performance scores on ACPT (d'), DCCS age adjusted score, fluid cognition composite score, Flanker age adjusted score and LSWS total score to compare across the diagnostic groups. A MANCOVA model consisting of these variables, controlled for diagnostic status, age, and sex, was significant (Wilk's $\lambda=0.66$, $F(14,280)=4.60$, $p<0.001$). Tests of between-subjects' effects showed that all except fluid cognition composite score were significantly different (all $p<0.001$). Post hoc Games-Howel-corrected tests showed that performance on all these tests except the fluid intelligence were significantly different between controls and NAP but not with AP patients. Only DCCS scores showed difference between AP and NAP patients.

First-order metrics: Partial correlations controlling for diagnostic status, age, and sex in the entire sample of patients and controls showed that left IP1 ($r=0.31$, $p<0.001$), left PH ($r=0.33$, $p<0.001$), and right POS2 ($r=0.27$, $p<0.001$) band power 5 were positively correlated with working memory after false discovery rate corrections. Posthoc correlations showed that performance on these cognitive tasks was significant within both patients and controls. Further, first-order metrics were not correlated with psychopathology severity.

Second-order metrics: None of the FC graph metrics correlated with cognitive test scores or psychopathology severity.

MEM-derived metrics: Partial correlation tests controlling for age, sex, and diagnostic status in the combined sample of patients and controls showed that DMN top ($r=-0.26$) and bottom ($r=-0.27$) basin transitions, DAN top basin transitions ($r=-0.21$), DMN+DAN top energy trace ($r=-0.22$), and DMN+DAN bottom basin transitions ($r=-0.22$) were significantly negatively correlated with working memory scores (all $p<0.004$) after false discovery rate corrections. MEM-derived metrics were not correlated with psychopathology severity.

4. Discussion

We contrasted the first-order, second-order, and MEM in examining regional differences in BOLD activation and FC features among early psychosis patients and controls, followed by examination of NAP and AP samples compared to controls from the HCP-EP dataset. We observed reductions in slow-5 frequency band power in multiple regions in patients compared to controls (**Table 1**) (**Supplemental Section 1.1**), supporting prior studies (26). These reductions co-occurred with increased binary brain state switching in DMN and DAN nodes (except bottom-switching DMN regions) (**Figure 8C**) that was explained by BOLD changes across DMN and DAN nodes **(Figure 8A)** (not the noise-bands), consistent with larger amplitude deflections driving microstate transitions. First-order results replicate prior findings using amplitude of low frequency fluctuations (ALFF) findings (33,56,57) and extend them by linking reduced band power to increased microstate switching.

Patients showed altered FC, with more anti-correlated DMN+DAN edges, weaker overall connections, lower clustering and efficiency, and higher modularity and betweenness centrality (**Figure 2; Supplemental Section 1.2**). Previous research points to patients having reduced brain-wide FC(9). These second-order findings suggest greater segregation with weaker local cohesion in patients, which is most evident in DMN+DAN, and less evident with either network studied alone. While psychosis patients had more anti-correlated functional connections between DMN and DAN compared to controls **(Figure 2; Supplemental Section S.2),** at the group average edge weight level, there were no detectable anti-correlations, likely due to the high individual variability of connectivity strength in these regions **(Figure 2)** (58).

In the MEM analysis, patients had more distinct binary states per system (**Figure 3**), particularly in top-switching systems where the group-level population distribution of energy traces was significantly higher in patients, which was not observed in the bottom switching systems (**Figure 4**). These findings demonstrate higher-energy, lower-probability brain states are more common and more often switching in psychosis, together suggesting that the resting networks may be relatively unstable in patients. Energy traces were lower in controls, indicating more stable states, whereas patients exhibited relatively more transient states, confirming prior results(59,60). Basin analysis (**Figure 5**) showed that all-on/all-off states are energy minima in all six systems, with additional DMN-only or DAN-only basins in DMN+DAN. Patients had more basin transitions in top-switching DMN, DAN, and DMN+DAN networks (**Figure 6**) and shorter dwell times in some basins but not different basin transition patterns (**Figure 7; Supplemental Section 1.4**), suggesting faster movement among higher-energy states

without altering transition architecture further supporting relative instability of selected functional networks.

In our examination of correlation of first-order, second-order, and MEM features with cognitive performance, we observed positive correlation of BOLD signal band power 5 of only three regions out of 58 with working memory. First-order-derived results only inform higher/lower BOLD strength averaged over the entire resting fMRI acquisition to correlate with cognitive functions that smooths out dynamic fluctuations in BOLD signals. Further, a higher or lower BOLD signals have been interpreted variously suggesting ambiguity in understanding the BOLD signal intensity levels(4,61). To partly address this limitation, we examined switching of brain states at each repetition time (TR) of fMRI acquisition. We observed that the top-switching DMN+DAN nodes consistently showed the most patient-control differences across first-order, second-order, and MEM features, whereas graph-level network measures did not, indicating MEM features preserve brain-behavior associations, as these associations were of similar strengths to that of recently published comparisons on the same sample(62). In addition, selected graph metrics calculated for the second-order models, did not correlate with cognitive performance suggesting their limited clinical significance.

The MEM formalizes system interactions consistent with neuroscience principles(63). It was initially used in cellular models of the retinal ganglion(64), hippocampal place cells(65), and primary visual cortex(66). More recently, the MEM has been implemented in the study of fMRI datasets(38,51,67-71). The model can be viewed as a generalization of the classic Ising model(72) into higher dimensional space that also includes a first-order term(73), expressing the likelihood of discrete states based on first- and second-order properties. Further MEM incorporates the non-independence (interdependence) of pairwise correlations unlike FC analysis where such correlations are assumed to be independent. This framework provides new quantities of interest from the signal over and above first-order-only or second-order-only statistics. Energy landscape analysis, which represents the global statistical structure of activation patterns over the length of fMRI acquisition, provides additional novel measures such as the basin structure and transition of distinct states. We show that the DMN, DAN, and DMN+DAN systems showed distinctly different structure of the landscape and transitions. We also find that most differences in these features were between NAP and controls, but not in AP-control and AP-NAP comparisons, which may partly be due to relatively smaller AP sample. In our prior study, we showed that bipolar disorder, major depressive disorder, and schizophrenia showed distinct states(59). In addition, transition rates and dwell time in the basins further enriches our understanding of the functional dynamics among psychosis patients, mostly contributed by non-affective psychosis.

Correlation with working memory but not other domains tested suggest that the MEM metrics from the resting fMRI data may be more specific to working memory. Our prior study showed the higher energy (low probability networks) were associated with executive functions when task-fMRI data was examined(51) suggesting that lack of association with measures of executive function, attention, and mental flexibility may be elicited in a task fMRI data. The correlated MEM metrics were primarily basin transitions in all three networks along with energy trace in DMN+DAN system. These findings suggest that the findings on MEM provides more nuanced and time-varying functional changes that may better represent inherently dynamic functional networks.

Lack of correlation with psychopathology was surprising. Our prior study using task fMRI data showed correlation of energy measures with total score on PANSS(51). Thus, it is possible that the MEM metrics derived from resting fMRI data may not be sensitive enough to show correlations with psychopathology severity.

The DMN has been well-established not just in human MRI but also through EEG (68) and in many other experimental contexts across the animal kingdom(74) and is evolutionarily conserved(75). The DAN is also highly evidenced in both human and animal studies(76,77). While speculative, their interaction could be related to the formation and maintenance of top-down attention constructs. For instance, competition between the DMN and DAN could produce a balance of internally-focused and externally-focused thoughts. While the DMN should be more prominent during rest, DAN activity during rest might help manage *which* internal thoughts are worth focusing on, and/or reciprocally the DMN is forming or pruning which stimuli merit attention(78). In plain terms, internal dialogues should inform goal orientation. Such a process would have explanatory value insofar as delusional thinking patterns (79) and/or disorganization of thought (80) may be a product of this interaction. Multiversal analysis, especially the inclusion of the MEM alongside established methods of brain regional and network studies, can help determine spatially localized and temporally resolved changes in brain state activity that are associated with cognitive impairments.

Funding Sources

This work was funded by the US National Institute of Mental Health (NIMH) through R01MH112584, R01MH115026, and R01MH137090 (KMP).

Acknowledgements

We want to thank the Pittsburgh Supercomputing Center for providing the computational resources through ACCESS Discover grant BIO200047.

Disclosures

The authors have nothing to disclose that is relevant for this manuscript.

References

1. O'Neill A, Mechelli A, Bhattacharyya S (2019): Dysconnectivity of Large-Scale Functional Networks in Early Psychosis: A Meta-analysis. *Schizophrenia bulletin*. 45:579–590.

2. Keshavan MS, Eack SM, Prasad KM, Haller CS, Cho RY (2017): Longitudinal functional brain imaging study in early course schizophrenia before and after cognitive enhancement therapy. *NeuroImage*. 151:55–64.
3. Stolz E, Pancholi KM, Goradia DD, Paul S, Keshavan MS, Nimgaonkar VL, et al. (2012): Brain activation patterns during visual episodic memory processing among first-degree relatives of schizophrenia subjects. *NeuroImage*. 63:1154–1161.
4. Glahn DC, Ragland JD, Abramoff A, Barrett J, Laird AR, Bearden CE, et al. (2005): Beyond hypofrontality: a quantitative meta-analysis of functional neuroimaging studies of working memory in schizophrenia. *Human brain mapping*. 25:60–69.
5. Ragland JD, Laird AR, Ranganath C, Blumenfeld RS, Gonzales SM, Glahn DC (2009): Prefrontal activation deficits during episodic memory in schizophrenia. *The American journal of psychiatry*. 166:863–874.
6. Cai M, Wang R, Liu M, Du X, Xue K, Ji Y, et al. (2022): Disrupted local functional connectivity in schizophrenia: An updated and extended meta-analysis. *Schizophrenia*. 8:93.
7. Steegen S, Tuerlinckx F, Gelman A, Vanpaemel W (2016): Increasing Transparency Through a Multiverse Analysis. *Perspect Psychol Sci*. 11:702–712.
8. Dafflon J, F. Da Costa P, Váša F, Monti RP, Bzdok D, Hellyer PJ, et al. (2022): A guided multiverse study of neuroimaging analyses. *Nature Communications*. 13:3758.
9. Voineskos AN, Hawco C, Neufeld NH, Turner JA, Ameis SH, Anticevic A, et al. (2024): Functional magnetic resonance imaging in schizophrenia: current evidence, methodological advances, limitations and future directions. *World Psychiatry*. 23:26–51.
10. Jacobs GR, Coleman MJ, Lewandowski KE, Pasternak O, Cetin-Karayumak S, Mesholam-Gately RI, et al. (2025): An Introduction to the Human Connectome Project for Early Psychosis. *Schizophrenia bulletin*. 51:658–671.
11. Zuo XN, Di Martino A, Kelly C, Shehzad ZE, Gee DG, Klein DF, et al. (2010): The oscillating brain: complex and reliable. *NeuroImage*. 49:1432–1445.
12. Epp SM, Castrillón G, Yuan B, Andrews-Hanna J, Preibisch C, Riedl V (2025): BOLD signal changes can oppose oxygen metabolism across the human cortex. *Nature neuroscience*.
13. Kennerley AJ, Harris S, Bruyns-Haylett M, Boorman L, Zheng Y, Jones M, et al. (2012): Early and late stimulus-evoked cortical hemodynamic responses provide insight into the neurogenic nature of neurovascular coupling. *Journal of cerebral blood flow and metabolism : official journal of the International Society of Cerebral Blood Flow and Metabolism*. 32:468–480.
14. Drew PJ (2019): Vascular and neural basis of the BOLD signal. *Curr Opin Neurobiol*. 58:61–69.
15. Penttonen M, Buzsáki G (2003): Natural logarithmic relationship between brain oscillators. *Thalamus & Related Systems*. 2:145–152.
16. Logothetis NK (2003): The Underpinnings of the BOLD Functional Magnetic Resonance Imaging Signal. *The Journal of Neuroscience*. 23:3963.
17. Gohel SR, Biswal BB (2015): Functional integration between brain regions at rest occurs in multiple-frequency bands. *Brain Connect*. 5:23–34.
18. Birn RM, Diamond JB, Smith MA, Bandettini PA (2006): Separating respiratory-variation-related fluctuations from neuronal-activity-related fluctuations in fMRI. *NeuroImage*. 31:1536–1548.

19. Moon HS, Jiang H, Vo TT, Jung WB, Vazquez AL, Kim SG (2021): Contribution of Excitatory and Inhibitory Neuronal Activity to BOLD fMRI. *Cereb Cortex*. 31:4053–4067.
20. Logothetis NK, Pauls J, Augath M, Trinath T, Oeltermann A (2001): Neurophysiological investigation of the basis of the fMRI signal. *Nature*. 412:150–157.
21. Magri C, Schridde U, Murayama Y, Panzeri S, Logothetis NK (2012): The Amplitude and Timing of the BOLD Signal Reflects the Relationship between Local Field Potential Power at Different Frequencies. *The Journal of Neuroscience*. 32:1395.
22. Bluhm RL, Miller J, Lanius RA, Osuch EA, Boksman K, Neufeld RW, et al. (2007): Spontaneous low-frequency fluctuations in the BOLD signal in schizophrenic patients: anomalies in the default network. *Schizophrenia bulletin*. 33:1004–1012.
23. Hirano Y, Oribe N, Kanba S, Onitsuka T, Nestor PG, Spencer KM (2015): Spontaneous Gamma Activity in Schizophrenia. *JAMA psychiatry*. 72:813–821.
24. Menon V (2023): 20 years of the default mode network: A review and synthesis. *Neuron*. 111:2469–2487.
25. Finn ES (2021): Is it time to put rest to rest? *Trends in cognitive sciences*. 25:1021–1032.
26. Garrity AG, Pearlson GD, McKiernan K, Lloyd D, Kiehl KA, Calhoun VD (2007): Aberrant "default mode" functional connectivity in schizophrenia. *The American journal of psychiatry*. 164:450–457.
27. Keane BP, Krekelberg B, Mill RD, Silverstein SM, Thompson JL, Serody MR, et al. (2023): Dorsal attention network activity during perceptual organization is distinct in schizophrenia and predictive of cognitive disorganization. *The European journal of neuroscience*. 57:458–478.
28. Bleuler E (1911): Dementia praecox or the group of schizophrenias.
29. Luck SJ, Gold JM (2008): The construct of attention in schizophrenia. *Biological psychiatry*. 64:34–39.
30. Esposito R, Cieri F, Chiacchiaretta P, Cera N, Lauriola M, Di Giannantonio M, et al. (2018): Modifications in resting state functional anticorrelation between default mode network and dorsal attention network: comparison among young adults, healthy elders and mild cognitive impairment patients. *Brain imaging and behavior*. 12:127–141.
31. Owens MM, Yuan D, Hahn S, Albaugh M, Allgaier N, Chaarani B, et al. (2020): Investigation of Psychiatric and Neuropsychological Correlates of Default Mode Network and Dorsal Attention Network Anticorrelation in Children. *Cereb Cortex*. 30:6083–6096.
32. Martin AK, Mowry B, Reutens D, Robinson GA (2015): Executive functioning in schizophrenia: Unique and shared variance with measures of fluid intelligence. *Brain Cogn*. 99:57–67.
33. Hoptman MJ, Zuo XN, Butler PD, Javitt DC, D'Angelo D, Mauro CJ, et al. (2010): Amplitude of low-frequency oscillations in schizophrenia: a resting state fMRI study. *Schizophrenia research*. 117:13–20.
34. Amaro E, Jr., Barker GJ (2006): Study design in fMRI: basic principles. *Brain Cogn*. 60:220–232.
35. Mohanty R, Sethares WA, Nair VA, Prabhakaran V (2020): Rethinking Measures of Functional Connectivity via Feature Extraction. *Scientific Reports*. 10:1298.

36. Reid AT, Headley DB, Mill RD, Sanchez-Romero R, Uddin LQ, Marinazzo D, et al. (2019): Advancing functional connectivity research from association to causation. *Nature neuroscience*. 22:1751–1760.
37. Masuda N, Islam S, Thu Aung S, Watanabe T (2025): Energy landscape analysis based on the Ising model: Tutorial review. *PLOS Complex Systems*. 2:e0000039.
38. Prasad K, Bowei O, Theis N (2025): From microstates to macroscales: A Critical Review of Maximum Entropy Modeling and Energy Landscape Analysis in functional MRI.
39. Glasser MF, Coalson TS, Robinson EC, Hacker CD, Harwell J, Yacoub E, et al. (2016): A multi-modal parcellation of human cerebral cortex. *Nature*. 536:171–178.
40. Ishida T, Yamada S, Yasuda K, Uenishi S, Tamaki A, Tabata M, et al. (2024): Aberrant brain dynamics of large-scale functional networks across schizophrenia and mood disorder. *NeuroImage: Clinical*. 41:103574.
41. Glasser MF, Sotiropoulos SN, Wilson JA, Coalson TS, Fischl B, Andersson JL, et al. (2013): The minimal preprocessing pipelines for the Human Connectome Project. *NeuroImage*. 80:105–124.
42. Buitrago P, Nystrom N (2021): Neocortex and Bridges-2: A High Performance AI+HPC Ecosystem for Science, Discovery, and Societal Good High Performance Computing, pp 205–219.
43. Fischl B (2012): FreeSurfer. *NeuroImage*. 62:774–781.
44. Jenkinson M, Beckmann CF, Behrens TE, Woolrich MW, Smith SM (2012): Fsl. *NeuroImage*. 62:782–790.
45. Holmes A, Levi PT, Chen YC, Chopra S, Aquino KM, Pang JC, et al. (2023): Disruptions of Hierarchical Cortical Organization in Early Psychosis and Schizophrenia. *Biol Psychiatry Cogn Neurosci Neuroimaging*. 8:1240–1250.
46. Lewis M, Theis N, Girish N, Prasad K (2025): Determining the atlas correspondence of Desikan-Killiany-Tourville and Glasser MMP1 atlases across magnetic field strengths. *Journal of neuroscience methods*. 418:110445.
47. Petersen SE, Seitzman BA, Nelson SM, Wig GS, Gordon EM (2024): Principles of cortical areas and their implications for neuroimaging. *Neuron*. 112:2837–2853.
48. Sandhu Z, Tanglay O, Young IM, Briggs RG, Bai MY, Larsen ML, et al. (2021): Parcellation-based anatomic modeling of the default mode network. *Brain Behav*. 11:e01976.
49. Allan PG, Briggs RG, Conner AK, O'Neal CM, Bonney PA, Maxwell BD, et al. (2019): Parcellation-based tractographic modeling of the dorsal attention network. *Brain Behav*. 9:e01365.
50. Rubinov M, Kötter R, Hagmann P, Sporns O (2009): Brain connectivity toolbox: a collection of complex network measurements and brain connectivity datasets. *NeuroImage*. 47:S169.
51. Theis N, Bahuguna J, Rubin JE, Banerjee SS, Muldoon B, Prasad KM (2025): Energy of Functional Brain States Correlates With Cognition in Adolescent-Onset Schizophrenia and Healthy Persons. *Human brain mapping*. 46:e70129.
52. Cho JW, Korchmaros A, Vogelstein JT, Milham MP, Xu T (2021): Impact of concatenating fMRI data on reliability for functional connectomics. *NeuroImage*. 226:117549.

53. Fu Z, Iraji A, Sui J, Calhoun VD (2021): Whole-Brain Functional Network Connectivity Abnormalities in Affective and Non-Affective Early Phase Psychosis. *Frontiers in Neuroscience*. Volume 15 - 2021.
54. Wang HR, Liu ZQ, Nakua H, Hegarty CE, Thies MB, Patel PK, et al. (2025): Decoding Early Psychoses: Unraveling Stable Microstructural Features Associated With Psychopathology Across Independent Cohorts. *Biological psychiatry*. 97:167–177.
55. O'Neill AG, Pax M, Parent JH, Sepulcre J, Camprodon JA, Noble S, et al. (2025): Predicting cognitive functioning in early psychosis: factors supporting and limiting generalizability of connectome-based models. *NPP—Digital Psychiatry and Neuroscience*. 3:11.
56. Meda SA, Wang Z, Ivleva EI, Poudyal G, Keshavan MS, Tamminga CA, et al. (2015): Frequency-Specific Neural Signatures of Spontaneous Low-Frequency Resting State Fluctuations in Psychosis: Evidence From Bipolar-Schizophrenia Network on Intermediate Phenotypes (B-SNIP) Consortium. *Schizophrenia bulletin*. 41:1336–1348.
57. Gohel S, Gallego JA, Robinson DG, DeRosse P, Biswal B, Szeszko PR (2018): Frequency specific resting state functional abnormalities in psychosis. *Human brain mapping*. 39:4509–4518.
58. Mueller S, Wang D, Fox MD, Yeo BT, Sepulcre J, Sabuncu MR, et al. (2013): Individual variability in functional connectivity architecture of the human brain. *Neuron*. 77:586–595.
59. Theis N, Bahuguna J, Rubin JE, Cape J, Iyengar S, Prasad KM (2024): Subject-specific maximum entropy model of resting state fMRI shows diagnostically distinct patterns of energy state distributions. *bioRxiv*.
60. Theis N, Bahuguna J, Rubin JE, Banerjee SS, Muldoon B, Prasad KM (2024): Energy of functional brain states correlates with cognition in adolescent-onset schizophrenia and healthy persons. *bioRxiv*.
61. Callicott JH, Mattay VS, Verchinski BA, Marenco S, Egan MF, Weinberger DR (2003): Complexity of prefrontal cortical dysfunction in schizophrenia: more than up or down. *The American journal of psychiatry*. 160:2209–2215.
62. Ward HB, Beermann A, Xie J, Yildiz G, Felix KM, Addington J, et al. (2025): Robust Brain Correlates of Cognitive Performance in Psychosis and Its Prodrome. *Biological psychiatry*. 97:139–147.
63. Savin C, Tkačik G (2017): Maximum entropy models as a tool for building precise neural controls. *Curr Opin Neurobiol*. 46:120–126.
64. Simoncelli EP, Olshausen BA (2001): Natural image statistics and neural representation. *Annu Rev Neurosci*. 24:1193–1216.
65. Fuhs MC, Touretzky DS (2006): A spin glass model of path integration in rat medial entorhinal cortex. *The Journal of neuroscience : the official journal of the Society for Neuroscience*. 26:4266–4276.
66. Tang A, Jackson D, Hobbs J, Chen W, Smith JL, Patel H, et al. (2008): A maximum entropy model applied to spatial and temporal correlations from cortical networks in vitro. *The Journal of neuroscience : the official journal of the Society for Neuroscience*. 28:505–518.
67. Watanabe T, Hirose S, Wada H, Imai Y, Machida T, Shirouzu I, et al. (2013): A pairwise maximum entropy model accurately describes resting-state human brain networks. *Nat Commun*. 4:1370.

68. Das A, de Los Angeles C, Menon V (2022): Electrophysiological foundations of the human default-mode network revealed by intracranial-EEG recordings during resting-state and cognition. *NeuroImage*. 250:118927.
69. Ezaki T, Watanabe T, Ohzeki M, Masuda N (2017): Energy landscape analysis of neuroimaging data. *Philos Trans A Math Phys Eng Sci*. 375:20160287.
70. Gu S, Cieslak M, Baird B, Muldoon SF, Grafton ST, Pasqualetti F, et al. (2018): The Energy Landscape of Neurophysiological Activity Implicit in Brain Network Structure. *Sci Rep*. 8:2507.
71. Kang J, Jeong SO, Pae C, Park HJ (2021): Bayesian estimation of maximum entropy model for individualized energy landscape analysis of brain state dynamics. *Human brain mapping*. 42:3411–3428.
72. Amit DJ, Gutfreund H, Sompolinsky H (1985): Spin-glass models of neural networks. *Phys Rev A Gen Phys*. 32:1007–1018.
73. Yeh F-C, Tang A, Hobbs JP, Hottowy P, Dabrowski W, Sher A, et al. (2010): Maximum Entropy Approaches to Living Neural Networks. *Entropy*. 12:89–106.
74. Pagani M, Gutierrez-Barragan D, de Guzman AE, Xu T, Gozzi A (2023): Mapping and comparing fMRI connectivity networks across species. *Commun Biol*. 6:1238.
75. Gutierrez-Barragan D, Ramirez JSB, Panzeri S, Xu T, Gozzi A (2024): Evolutionarily conserved fMRI network dynamics in the mouse, macaque, and human brain. *Nat Commun*. 15:8518.
76. Corbetta M, Shulman GL (2002): Control of goal-directed and stimulus-driven attention in the brain. *Nature Reviews Neuroscience*. 3:201–215.
77. Fox MD, Corbetta M, Snyder AZ, Vincent JL, Raichle ME (2006): Spontaneous neuronal activity distinguishes human dorsal and ventral attention systems. *Proceedings of the National Academy of Sciences*. 103:10046–10051.
78. Spreng RN, Stevens WD, Chamberlain JP, Gilmore AW, Schacter DL (2010): Default network activity, coupled with the frontoparietal control network, supports goal-directed cognition. *NeuroImage*. 53:303–317.
79. Lavigne KM, Menon M, Woodward TS (2020): Functional Brain Networks Underlying Evidence Integration and Delusions in Schizophrenia. *Schizophrenia bulletin*. 46:175–183.
80. Hur JW, Kim T, Cho KIK, Kwon JS (2021): Attenuated Resting-State Functional Anticorrelation between Attention and Executive Control Networks in Schizotypal Personality Disorder. *J Clin Med*. 10.